Check for updates

Chemistry Europe
European Chemical Societies Publishing

Origin of the Rate Acceleration in the C–C Reductive Elimination from Pt(IV)-complex in a $[Ga_4L_6]^{12-}$ Supramolecular Metallocage

Gantulga Norjmaa,[a] Jean-Didier Maréchal,*[a] and Gregori Ujaque*[a]

Abstract: The reductive elimination on $[(Me_3P)_2Pt(MeOH)(CH_3)_3]^+$, **2P**, complex performed in MeOH solution and inside a $[Ga_4L_6]^{12-}$ metallocage are computationally analysed by mean of QM and MD simulations and compared with the mechanism of gold parent systems previously reported $[Et_3PAu(MeOH)(CH_3)_2]^+$, **2Au**. The comparative analysis between the encapsulated Au(III) and Pt(IV)-counterparts shows that there are no additional solvent MeOH molecules inside the cavity of the metallocage for both systems. The Gibbs energy barriers for the **2P** reductive elimination calculated at DFT level are in good agreement with the experimental values for both environments. The effect of microsolvation and encapsulation on the rate acceleration are evaluated and shows that the latter is far more relevant, conversely to **2Au**. Energy decomposition analysis indicates that the encapsulation is the main responsible for most of the energy barrier reduction. Microsolvation and encapsulation effects are not equally contributing for both metal systems and consequently, the reasons of the rate acceleration are not the same for both metallic systems despite the similarity between them.

Introduction

Supramolecular catalysis is an interesting discipline that combines catalysis and supramolecular chemistry.[1–8] In the last few decades, several supramolecules have been designed as microenvironments for chemical reactions and applied to the host-guest catalysis, with metal–organic cages (MOCs) playing a prominent role.[9–12] Metal–organic cages (M_xL_y), also named supramolecular organometallic cages (SOCs) or metallocages,[13] are prepared from metal ions and organic ligands and have well defined cavities in size and shape; they are able to host molecules or ions and chemical reactions.[14,15] Examples are Raymond's Ga_4L_6,[16] Fujita's Pd_6L_4,[17] Nitschke's Fe_4L_6,[18] Lusby's Pd_2L_4,[19] among others.[20,21]

The metallocage $K_{12}[Ga_4L_6]$ developed by Raymond and coworkers has been successfully applied to accelerate many reactions: alkyl-alkyl reductive elimination,[22] orthoformate hydrolysis,[23] Nazarov cyclization,[24] hydroalkylation,[25] etc.[26–28] Among these reactions, the alkyl-alkyl reductive elimination has been studied in detail for high valent transition metal complexes (Au(III) and Pt(IV) complexes) by Bergman, Raymond and Toste groups.[22,29] The reaction from Au(III) complexes was also computationally investigated by us,[30,31] and by Head-Gordon group.[32,33] For the case of Pt(IV) a computational mechanistic analysis on the origin of rate enhancement is missing. A general scheme on the processes here investigated are shown in Scheme 1.

Theoretical studies are essential to understand catalytic processes;[34–37] however, computational works on supramolecular catalysis are still scarce.[38–47] In the case of highly anionic hosts, as the $[Ga_4L_6]^{12-}$ metallocage, all computational studies show that electrostatic effects are crucial for the rate acceleration.[30–33,48,49] In our previous works, we studied the reductive eliminations from the Au(III) complexes, $[R_3PAu(MeOH)(CH_3)_2]^+$, in the $[Ga_4L_6]^{12-}$ and showed that not only encapsulation by the host, but also microsolvation plays an important role for lowering the Gibbs energy barrier of the reductive elimination from the Au(III) complexes inside $[Ga_4L_6]^{12-}$.[30,31]

In the present study, we investigate computationally the origin of the catalysis observed for alkyl-alkyl reductive elimination from the Pt(IV)-complex, [*trans*-$(Me_3P)_2Pt(MeOH)(CH_3)_3]^+$, **2P**. The analysis is performed first in solution and then inside the metallocage, $[Ga_4L_6]^{12-}$, **3**, (Scheme 1). Microsolvation and encapsulation effects on the reduction of the Gibbs energy barrier in the metallocage are analysed. Moreover, comparisons of the encapsulation effects of the $[Ga_4L_6]^{12-}$ metallocage on the Au(III) and the Pt(IV) reductive elimination processes are performed. This could lead to significant contribution in both understanding and developing chemical reactions in confined space.

[a] *G. Norjmaa, Dr. J.-D. Maréchal, Dr. G. Ujaque*
Departament de Química and Centro de Innovación en Química Avanzada (ORFEO-CINQA)
Universitat Autònoma de Barcelona
08193 Cerdanyola del Valles, Barcelona, Catalonia (Spain)
E-mail: jeandidier.marechal@uab.cat
gregori.ujaque@uab.cat

Supporting information for this article is available on the WWW under https://doi.org/10.1002/chem.202102250

© 2021 The Authors. Chemistry - A European Journal published by Wiley-VCH GmbH. This is an open access article under the terms of the Creative Commons Attribution Non-Commercial License, which permits use, distribution and reproduction in any medium, provided the original work is properly cited and is not used for commercial purposes.

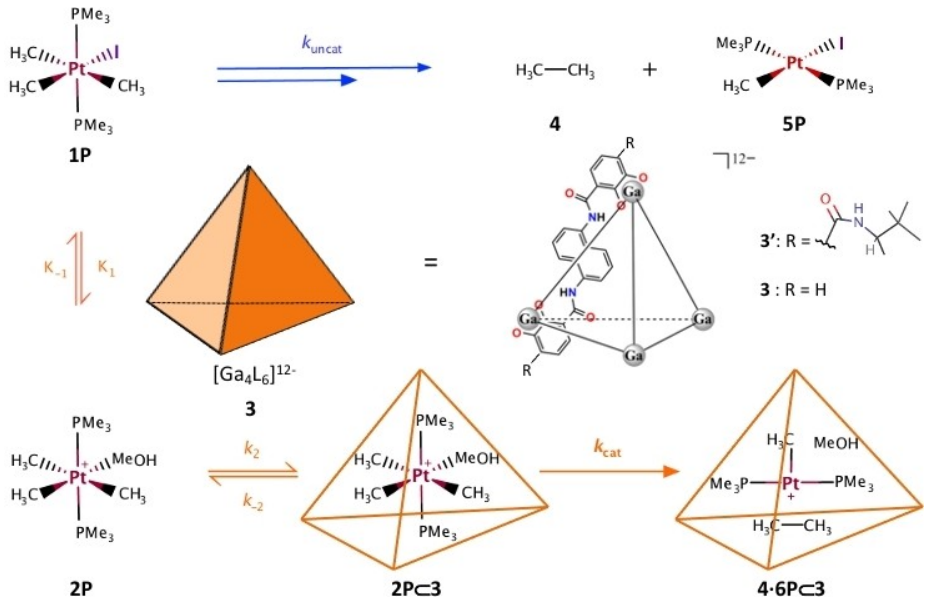

Scheme 1. Schematic representation of reductive elimination from [*trans*-$(Me_3P)_2Pt(I)(CH_3)_3$] complex, **1P**. Reaction in MeOH solution (blue arrow) and inside $[Ga_4L_6]^{12-}$ metallocage **3**, (orange arrow).

Results and Discussion

The alkyl-alkyl reductive elimination from the Pt(IV) complexes provide a rich ensemble of experimental data. First, in terms of catalysis, the reaction is highly accelerated in the presence of metallocage, $[Ga_4L_6]^{12-}$, **3** although the catalytic profile is function of the isomer. For *cis*-$[(Me_3P)_2PtI(CH_3)_3]$, the measured rate constant, k_{cat}, is $2.4\times10^{-2}\ s^{-1}$, with an acceleration (k_{cat}/k_{uncat}) of 2.6×10^4 for the encapsulated system.[22] For *trans*-$[(Me_3P)_2PtI(CH_3)_3]$ complex, the process inside the $[Ga_4L_6]^{12-}$ was too fast at the catalytically relevant temperature (45 °C) for accurate monitoring by ^1H NMR; nevertheless, at 25 °C the measured rate constant was $2.0\times10^{-2}\ s^{-1}$.[29] Experiments also indicate that the complex needs to become positively charged, thus losing the iodide ligand, to be encapsulated by the metallocage **3**. Such phenomenon is not observed in the absence of the metallocage. Finally, experimental observations also suggest that the *trans*-isomer of the Pt(IV) cationic complex, **2P**, is the one involved in the catalytic cycle for generating the C–C bond, whereas the *cis*-isomer, **cis2P**, is an off-cycle resting state (Figure 1). Based on these experimental evidences we decided to perform the comparative analysis for the reductive elimination in solution and inside the metallocage on the *trans*-Pt(IV) isomer.

Considering the experimental data exposed previously our working methodology consists in: 1) studying the reaction in solution, 2) studying the reaction in the metallocage, 3) investigating the origin of the rate acceleration within the metallocage compared to that in solution, and finally 4) comparative analysis on the origin of the catalysis between the Pt(IV) and the Au(III)-counterparts.

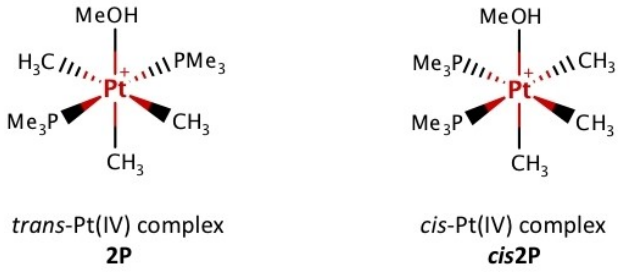

Figure 1. *Cis*- and *trans*- isomers of cationic Pt(IV) complex, $[(Me_3P)_2\mathbf{Pt}(MeOH)(CH_3)_3]^+$.

Reaction in solution

To investigate the catalytic properties of the metallocage, the reaction was initially evaluated in solution. The reaction inside the metallocage takes place through the cationic complex once the iodide is released. For the sake of comparison, the reaction is solution was analysed for both the neutral and cationic complexes (and both *cis* and *trans* isomers).

The reductive elimination from the *cis*-$[(Me_3P)_2PtI(CH_3)_3]$, **cis1P**, complex was first evaluated because this process can be directly compared with experiment (Figure 2). The measured rate constant of $9.2\times10^{-7}\ s^{-1}$ at 40 °C in MeOH solution, corresponds to a Gibbs energy barrier of 27.0 kcal/mol. The calculated Gibbs energy barrier for the reductive elimination step for the **cis1P** complex in solution is 28.7 kcal/mol (the iodide ligand is non-coordinated at the transition state, with a $Pt\cdots I^-$ distance of 4.5 Å). Nevertheless, the reaction is supposed to go through the formation a cationic species by losing the iodide ligand. Two complexes may be formed, a penta-coordinated complex *cis*-$[(Me_3P)_2Pt(CH_3)_3]^+$, **cis1P-I**, or the solvento complex *cis*-$[(Me_3P)_2Pt(MeOH)(CH_3)_3]^+$, **cis2P**. The rela-

© 2021 The Authors. Chemistry - A European Journal published by Wiley-VCH GmbH

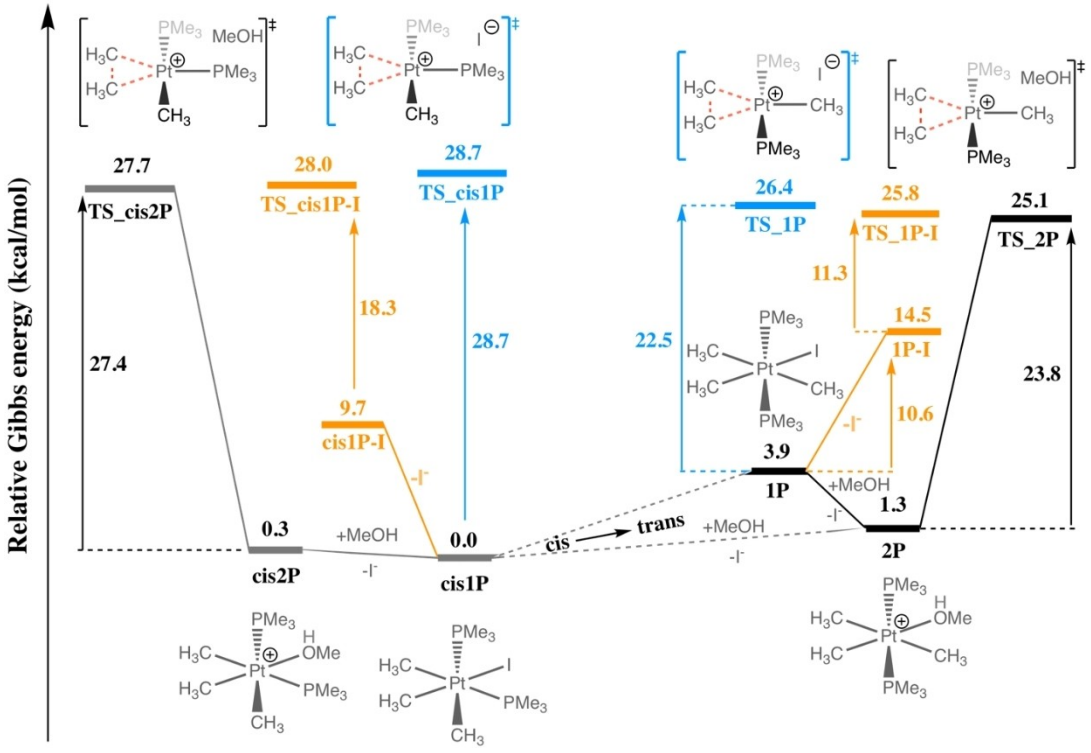

Figure 2. Gibbs energy profiles of reductive eliminations from *cis*- and *trans*-Pt(IV) species in solution.

tive Gibbs energy value for the formation of **cis1P-I** complex is 9.7 kcal/mol. Nevertheless, such a penta-coordinated complex is not stable. The inclusion of explicit solvent molecules in the calculation, a MeOH molecule, shows a spontaneous binding to the metal species forming the solvento complex **cis2P**, with a relative energy of 0.3 kcal/mol. The reductive elimination from this intermediate has a relative Gibbs energy barrier of 27.4 kcal/mol.

To evaluate microsolvation for this process, we calculated the Gibbs energy barrier for the reductive elimination process including additional solvent molecules explicitly. For the case of the solvento complex with an additional MeOH hydrogen-bonding the coordinated one, complex **cis2P-2**, the Gibbs energy barrier slightly decreases to 26.9 kcal/mol. The Gibbs energy barrier was also calculated for the systems including three, **cis2P-3**, four, **cis2P-4** and five, **cis2P-5** explicit solvent molecules. The values obtained are 26.3, 25.4 and 26.9 kcal/mol, for transition states **TS_cis2P-3**, **TS_cis2P-4** and **TS_cis2P-5**, respectively (Table 1). These barriers are quite similar and they converge once the solvento complex is considered. Thus, including the coordinated solvent molecule along with the continuum model nicely reproduces the experimental value for the reductive elimination barrier; no additional solvent molecules need to be considered. Indeed, calculated barriers range from 25.4 to 27.4 kcal/mol, in excellent agreement with experimental value of 27.0 kcal/mol.

Table 1. Gibbs energy barrier for the reductive elimination as a function of solvent molecules included in the model (in kcal/mol).

Explicit solvent molecules	*Cis*-isomer of Pt(IV)	*Trans*-isomer of Pt(IV)
0 (penta coordinated)	18.3	11.7
1	27.4	23.8
2	26.9	26.3
3	26.3	24.4
4	25.4	24.4
5	26.9	24.3

The reductive elimination from complex *trans*-[$(Me_3P)_2PtI(CH_3)_3$], **1P**, was also analysed (Figure 2). **1P** has a relative Gibbs energy of 3.9 kcal/mol compared to **cis1P**, with an energy barrier for the direct reductive elimination of 22.5 kcal/mol. This complex loses the iodide ligand and can potentially form two intermediates: a penta-coordinated complex *trans*-[$(Me_3P)_2Pt(CH_3)_3]^+$, **1P-I**, or the solvento complex *trans*-[$(Me_3P)_2Pt(MeOH)(CH_3)_3]^+$, **2P**. Their relative energies are 14.5 and 1.3 kcal/mol, respectively, compared to the most stable complex, **cis1P**. Once again, the penta-coordinated complex, **1P-I**, is not stable: a MeOH molecule spontaneously binds the metal species forming **2P**. The relative Gibbs energy of **2P** and **cis2P** complexes are 1.3 and 0.3 kcal/mol, respectively. The reductive elimination was calculated from intermediate **2P** with a relative Gibbs energy barrier of 23.8 kcal/mol, **TS_2P**. Inclusion of another explicit solvent MeOH, forming species **2P-2**, it gives rise to a Gibbs energy barrier of 26.3 kcal/mol, **TS_2P-2**. The values obtained for the Gibbs energy barriers including additional solvent molecules are 24.4, 24.4 and 24.3 kcal/mol, for **TS_2P-3**, four, **TS_2P-4** and five, **TS_2P-5**, respectively (Table 1). In agreement with the *cis* isomers, these results illustrate that microsolvation effects are not significantly contributing to the

© 2021 The Authors. Chemistry - A European Journal published by Wiley-VCH GmbH

reduction of Gibbs energy barrier once the solvento complex is considered. As far as the *cis*- and *trans*- complexes are affecting the reductive elimination itself, all the barriers for the *cis* complex are ~5 kcal/mol systematically higher than their analogous *trans* complexes (i.e. **TS_cis2P** vs. **TS_2P** corresponds to 27.4 vs. 23.8 kcal/mol, or **TS_cis1P** vs. **TS_1P** corresponds to 28.7 vs. 22.5 kcal/mol, respectively). Therefore, the *trans* isomer is always favoured for the reductive elimination over the *cis* isomer. This is in line with the fact that the *trans* isomer is the one involved in the catalytic reaction inside the metallocage (see below).

The optimized geometries of the transition states for *cis* and *trans* species are shown in Figure 3. In the transition states, $\mathbf{TS}_{\mathbf{2P\text{-}2}}$, and $\mathbf{TS}_{\mathit{cis}\mathbf{2P\text{-}2}}$, the forming C–C bond distances are 2.03 Å and 2.06 Å, showing that the forming C–C bond distances are quite similar for both *trans*- and *cis*-isomers of the Pt(IV) complex. Regarding the effect of microsolvation in the geometries, for transition state, **TS_2P**, the forming C–C bond distance is 2.04 Å compared to that of 2.03 Å for the **TS_2P-2**. This indicates that microsolvation does not significantly modify the C–C forming bond distance at the transition state. Similar behaviour is found when comparing **TS_cis2P-2** and **TS_cis2P-5** geometries with 2 and 5 solvent molecules explicitly included. Overall, microsolvation effects are not playing a significant role in the geometry of the reductive elimination transition states for *cis* and *trans* isomers, once the solvento complex is considered.

These results contrast with what was found for Au(III) complexes. The reductive elimination of the Au(III) complex analysed in our previous work,[30] showed that microsolvation is crucial. In fact, it was found that by removing explicit solvent molecules around the complex the barrier can diminish by up to 5.7 kcal/mol. As far as for geometries is concerned, for the case of Au(III) complex, microsolvation does not modifies the geometries significantly. All these results show that microsolvation is playing a very different role depending on the process considered. Thus, its effect on the octahedral Pt(IV) complex is nearly irrelevant, whereas the effect on the square planar Au(III) complex is decisive.

Reaction inside the metallocage

As previously commented, for the reaction taking place inside the $[Ga_4L_6]^{12-}$ metallocage **3** it is assumed that the *trans* isomer is the one involved in the catalytic cycle. Thus, we performed the computational analysis on the encapsulated *trans* isomer of the Pt complex, **2P**.

First, we performed classical molecular dynamic (MD) simulation of **2P** complex inside metallocage, **3**, (**2P**⊂**3**).[50] Classical MD simulations were carried out within a periodic box of explicit solvent MeOH molecules. The simulation of the host-guest complex, **2P**⊂**3**, shows that there are no solvent MeOH molecules inside the metallocage along with **2P** complex during the simulation time (over 100 ns; Figure S1). This suggests that **2P** fills in the cavity of the metallocage without availability for accommodating additional solvent molecules. In fact, the packing coefficient of 59% is calculated for the optimized structure of the **2P**⊂**3** complex, which is consistent with the Rebek's 55% rule.

The reductive elimination process inside the metallocage was computed at DFT-D3 level using the host-guest complex, **2P**⊂**3**. This system was selected based on the MD simulations: they indicate that no additional solvent molecules are encapsulated. The calculated Gibbs energy barrier is 17.3 kcal/mol (Figure 4, green profile), in very good agreement with the estimated value of 19.8 kcal/mol from the experimental rate constant of $2.0 \cdot 10^{-2}$ s^{-1} at 25 °C.[29]

A comparison of the Gibbs energy barrier of the reductive elimination in solution (24.3 kcal/mol for $\mathbf{TS}_{\mathbf{2P\text{-}5}}$) and inside the metallocage (17.3 kcal/mol for $\mathbf{TS}_{\mathbf{2P}\subset\mathbf{3}}$), shows that the overall reduction is 7.0 kcal/mol. The effect of performing the reductive elimination within the metallocage is huge. To gain understanding on the process, the microsolvation and encapsulation effects on the barrier decrease were analysed in detail (Figure 4; Table S2). As described in the previous section microsolvation effects are rather low. They are obtained by computing the Gibbs energy difference between the process in solution, by considering explicit solvent molecules surrounding the metal complex, and the analogous process by removing explicit solvent molecules (always accounting for solvent effects by a continuum method). Their Gibbs energy barriers are 24.3 kcal/

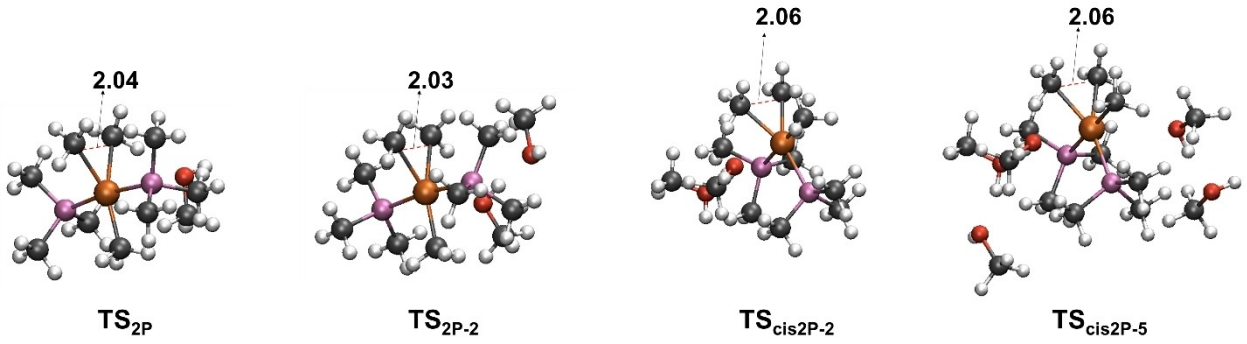

Figure 3. Optimized geometries of the transition states of reductive eliminations from **2P**, **2P-2**, ***cis*2P-2** and ***cis*2P-5**. Bond distances are in Å. Color code: Pt in brown, P in pink, C in gray, O is in red, and H in white.

© 2021 The Authors. Chemistry - A European Journal published by Wiley-VCH GmbH

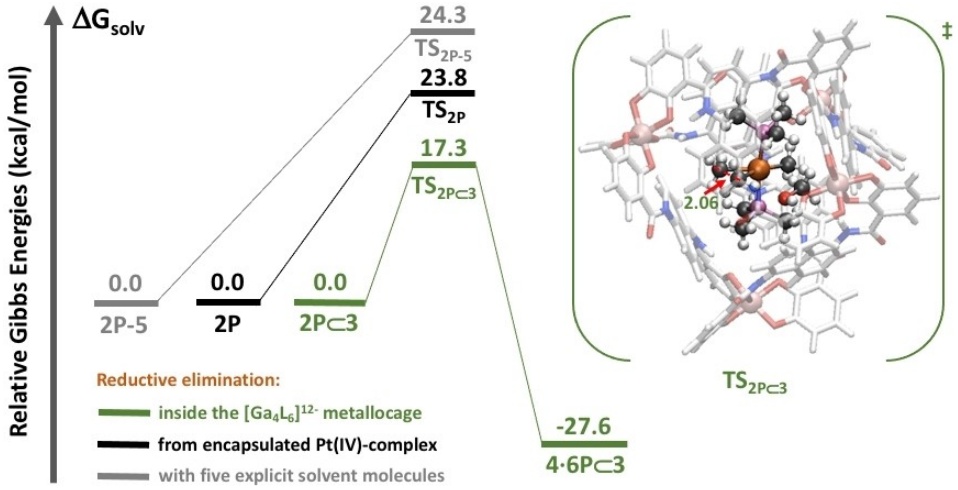

Figure 4. Gibbs energy profiles (in kcal/mol) for the reductive elimination in solution and inside metallocage.

mol, **TS_2P-5**, and 23.8 kcal/mol, **TS_2P**, respectively (both shown in Figure 4). Therefore, microsolvation effects account for a decrease of the Gibbs energy barrier of only 0.5 kcal/mol. The encapsulation effect can be obtained by comparing the Gibbs energy barrier for the reductive elimination of the "naked" solvento complex in solution, **TS_2P**, and inside the metallocage, **TS_2P⊂3**. The barrier decreases by as much as 6.5 kcal/mol. These results illustrate that microsolvation effects are small whereas encapsulation effects are the major contributors to the overall Gibbs energy decrease.

As far as for the geometrical parameters is concerned, the geometry of the transition state encapsulated in the metallocage is illustrated in Figure 4. The forming C–C bond distance in the transition state, $TS_{2P\subset 3}$, is 2.06 Å; this value is very similar to that for the transition state in solution, TS_{2P}, of 2.04 Å (Figure 3). This evidences that the forming bond distance is not significantly affected by encapsulation. The other metal ligand distances are not significantly modified either.

The Gibbs energy barrier is computed by adding thermal corrections (roughly related to the entropic term) to the potential energy (closely related to the enthalpic term). The thermal correction for the process in solution is −2.2 kcal/mol, whereas it is −1.0 kcal/mol for the encapsulated process. Therefore, thermal effects are rather similar in both environments, although the reduction of the barrier is slightly lower inside the cavity by 1.2 kcal/mol. Overall, these results suggest that thermal effects are not playing a significant role upon encapsulation.

As far as the potential energy is concerned, the calculated barrier is highly affected by encapsulation by as much as 7.7 kcal/mol. This magnitude can be analysed in terms of strain and interaction energies. In solution, the potential energy barrier is 26.0 kcal/mol (**2P**→**TS_2P**; black line in Figure 5). The

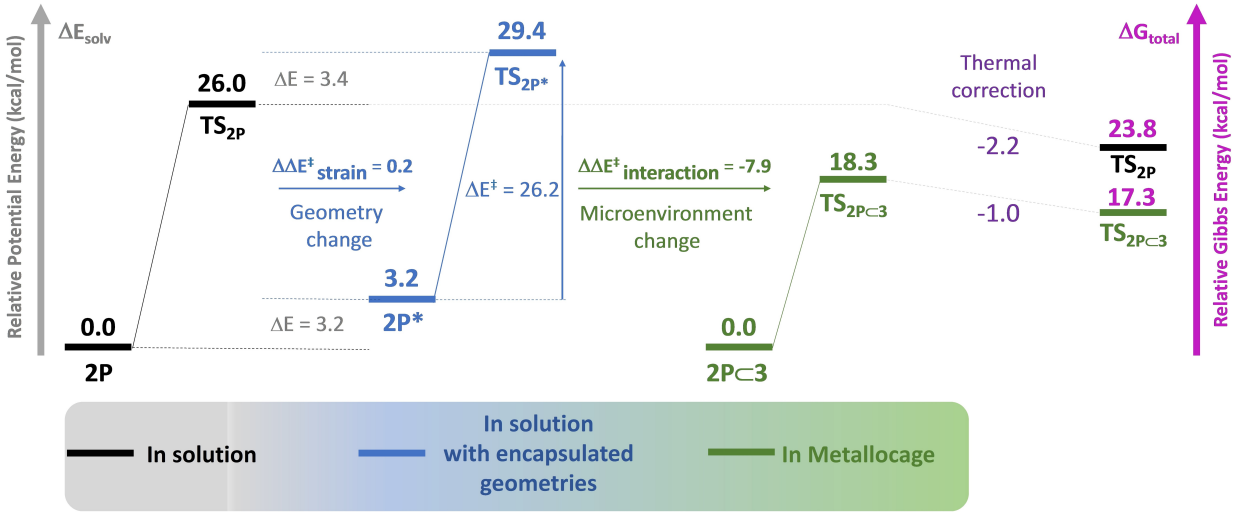

Figure 5. Decomposition analysis of Gibbs energy and potential energy barriers for the process in solution and inside the metallocage. Energies in kcal/mol.

© 2021 The Authors. Chemistry - A European Journal published by Wiley-VCH GmbH

barrier for the process calculated in solution taking frozen geometries of the encapsulated reactant (**2P***) and the encapsulated transition state ($\mathbf{TS_{2P*}}$), and considering solvent effects by continuum model (**2P*→TS_2P***), is 26.2 kcal/mol (blue line in Figure 5). This barrier is very similar to the one obtained in solution 26.0 kcal/mol. This is because the reactant and transition state are both similarly strained upon encapsulation: reactant is strained by 3.2 kcal/mol (**2P→2P***), whereas the transition state is strained by 3.4 kcal/mol, (**TS_2P→TS_2P***), respectively. Therefore, the overall strain effect is negligible. This means that the effect of the metallocage on the geometry modification along the reaction is practically insignificant ($\Delta\Delta E^{+}_{strain} = 0.2$ kcal/mol).

The potential energy barrier calculated for the encapsulated process, **2P⊂3→ TS_2P⊂3**, is 18.3 kcal/mol (green line in Figure 5). These results indicate that the reductive elimination from the Pt(IV) complex **2P** is reduced by 7.9 kcal/mol upon encapsulation. Therefore, encapsulation accounts for the largest influence in reducing the barrier. When considering strain (0.2 kcal/mol) and interaction (-7.9 kcal/mol) energies together, the potential energy barrier for the process is reduced by 7.7 kcal/mol (from 26.0 to 18.3, Figure 5). A summary of the decomposition analysis of the reduction of the Gibbs energy barrier over encapsulation is presented in Table S2.

A non-covalent interaction (NCI)[51,52] analysis of the encapsulated reactant, **2P⊂3**, and transition state, **TS 2P⊂3**, shows that the greatest differences between both structures come from the interaction with the coordinated MeOH solvent molecule. In the TS such a molecule is not bonded to the metal thus becoming available to attractively interact with the metallocage through one of the oxygens of the metallocage (H···O acceptor distance of 1.84 Å; Figure S2). Such an interaction is missing in the reactant. Moreover, the Me ligands involved in the forming C–C bond interact slightly strongerly with one of the naphthalene rings of the metallocage than when they are pure Me ligands in the reactant state.

We also performed a comparative analysis among the results for Pt(IV) complex (here studied) and Au(III) complex (studied in a previous work).[30] The Gibbs energy barrier reduction for the encapsulated process in the case of Au(III) complex, $[(Et_3P)Au(MeOH)(CH_3)_2]^+$, is 8.8 kcal/mol, whereas that for Pt(IV) complex, *trans*-$[(Me_3P)_2Pt(MeOH)(CH_3)_3]^+$, is 7.0 kcal/mol. Both complexes are equally positively charged, +1, and the barrier decrease is relatively similar, though slightly larger for the Au(III) complex. We explored if the origin of the reduction on the barrier is analogous for both complexes.

The MD simulations of the encapsulated complexes show that there are no additional solvent molecules inside the cavity for any of them. Therefore, in both cases the solvento complex becomes "naked" inside the metallocage. The microsolvation for the Au(III) complex was computed to be 5.7 kcal/mol, whereas that for Pt(IV) is 0.5 kcal/mol. Hence, microsolvation is very different for both metallic complexes. Note that this is a feature that depends on the reaction itself, not on the nature of the metallocage. As far as encapsulation is concerned, the Gibbs energy barrier decrease for the case of Au(III) was calculated to be 3.1 kcal/mol, whereas for Pt(IV) is 6.5 kcal/mol. Thus, the effect of the metallocage is larger for Pt(IV) than for Au(III) by 3.4 kcal/mol. Overall, microsolvation effects are much larger in the case of Au(III), whereas encapsulation effects are larger for the case of Pt(IV) complex.

We performed a comparative analysis in terms of potential energy and thermal correction magnitudes. Comparison of the thermal correction term in solution and encapsulated processes shows different trends for both metal complexes. In solution, thermal corrections are rather similar for both the Pt(IV) complex (−2.2 kcal/mol; Figure 5) and the Au(III) complex (−3.0 kcal/mol).[30] Inside the metallocage they are calculated to be −1.0 kcal/mol for the Pt(IV) complex (Figure 5), favouring the reaction, whereas they are 1.7 kcal/mol for the Au(III) complex, disfavouring the reaction. Anticipating the sign of the thermal contributions is therefore quite difficult even for similar processes.

Further energy decomposition analysis of the potential energy allows identifying the strain and interaction energies associated. Contributions from the strain term to the reduction of energy barrier for both complexes are 0.2 kcal/mol for Pt(IV) (Figure 5) and 1.2 kcal/mol for Au(III) complexes, respectively. The strain term is nearly negligible for both complexes. The interaction term is calculated to be −7.9 kcal/mol for Pt(IV) complex (Figure 5), and −9.0 kcal/mol for the Au(III) complex, respectively. It is the most important term and similar to both complexes. Interestingly, Pt(IV) and Au(III) complexes have a very different geometry (octahedral and square planar, respectively), but the interaction energy is similar for both cases. This reveals that the shape of the complex may not be so relevant for the encapsulated process. Overall, the effect of the metallocage environment on the potential energy is crucial for diminishing the barrier for both processes.

In summary, the contribution of microsolvation and encapsulation terms to diminishing the Gibbs energy barrier are not similar for both complexes. Whereas microsolvation is the most important contribution for Au(III) complex, for Pt(IV) it is by far the encapsulation term. Regarding the energy decomposition analysis, it shows that the strain term is negligible for both complexes, whereas the interaction term is clearly the most important one. This agrees with previous works on related processes.[32,33,49]

Conclusions

The observed rate acceleration of the alkyl-alkyl reductive elimination from the Pt(IV) complex encapsulated in the $[Ga_4L_6]^{12-}$ supramolecular metallocage is examined by means of computational calculations. The reaction is analysed in MeOH solution and inside $[Ga_4L_6]^{12-}$ metallocage **3**. The reaction in solution is investigated for *cis*- and *trans*-$[(Me_3P)_2Pt(MeOH)(CH_3)_3]^+$, **cis2P** and **2P**, complexes, respectively. For both complexes, the formation of the pentacoordinated structure (by losing the iodide ligand) was found to be not stable, instead, the solvento complex was spontaneously formed. The Gibbs energy barriers from the *trans* and *cis* isomers of the solvento complex (**2P** and **cis2P**) are very similar whose values are 24.3

© 2021 The Authors. Chemistry - A European Journal published by Wiley-VCH GmbH

and 26.9 kcal/mol, respectively. They are in very good agreement with the experimental value of 27.0 kcal/mol for the *cis* complex.

The reaction inside the metallocage was evaluated for the *trans* complex, **2P⊂3**. The MD simulations show that there are no additional solvent molecules inside the cage (apart from that coordinated to the metal complex). The Gibbs energy barrier for the reductive elimination was found to be 17.3 kcal/mol, in very good agreement with experimental value of 19.8 kcal/mol. The analysis of microsolvation and encapsulation effects show that whereas the first is very low (0.5 kcal/mol), the latter is crucial (6.5 kcal/mol). Energy decomposition analysis, in turn, show that the interaction energy (between the metallocage and the solvento complex) is by far the most important contribution, in agreement with other proposals.[32,33,49] The contribution of strain energies, in turn, are nearly negligible.

The comparative analysis between octahedral Pt(IV) complex and the square planar Au(III) complex show that the decrease of the Gibbs energy barrier for the encapsulated reaction is similar, by 7.0 and 8.8 kcal/mol, respectively. The contribution of microsolvation and encapsulation terms, however, are not analogous: whereas microsolvation is the most important contribution for Au(III) complex (with a relevant contribution of encapsulation too), for Pt(IV) it is the encapsulation the most important term (with a slight contribution of the microsolvation term). The comparative energy decomposition analysis show that strain is negligible whereas interaction with the metallocage is very similar for both metal complexes, despite having different geometries (octahedral and square-planar, respectively). Revealing these similarities and differences in the origin of such host-guest catalysis should lead to deeper understanding of this catalysis and help to develop chemical reactions in confined space.

Experimental Section

Computational details

The calculations were performed using the B3LYP-D3 functional[53–55] as implemented in the Gaussian 09 program.[56] All stationary points were characterized by frequency calculations. All calculations were performed with the 6-31G(d) basis set for the main group elements and SDD pseudopotential complemented with a set of *d* and *f* polarization functions for the gallium and the platinum atoms, respectively.[57,58] Solvation effects were included in all calculations using the SMD polarizable continuum model (e = 32.613, methanol as solvent).[59] The quasi-rigid-rotor-harmonic-oscillator (*quasi*-RRHO) approach was applied to correct the thermal effects.[60] Three-body DFT-D3 dispersion corrections,[55] and the standard state corrections (1.9 kcal/mol to each of the compounds except for methanol, 3.8 kcal/mol)[61] to the Gibbs energies were also added separately (Table S3).

Classical molecular dynamic simulations were performed using Amber 16 program.[62] To generate parameters for the platinum center, a python based metal center parameter builder (MCPB.py)[63] was employed whereas the antechamber was used for the RESP charge derivation of the platinum complex.[64,65] The parameters and charges of the metallocage were derived in our previous work and applied directly in the present study.[30,31,66] The rest of the parameters were taken from a general AMBER force field.[67] The simulations were performed under isothermal-isobaric (NPT) conditions (P = 1 bar, T = 298.15 K) with a periodic box of 68 Å × 68 Å × 68 Å (MEOHBOX) including 11 K^+ counter ions; this corresponds to approximately experimental concentration of the metallocage in solution (5 mM). To determine solvent MeOH molecules in the cavity, the last 100 ns were considered from a production phase of 160 ns after an equilibration period of 60 ns.

Acknowledgements

The authors acknowledge the financial support of the Spanish MINECO-FEDER (Grants CTQ2017-87889-P and PID2020-116861GB-I00). UAB is also acknowledged by a PIF grant to G. N.

Conflict of Interest

The authors declare no conflict of interest.

Keywords: density functional theory · metallocage · molecular dynamics · platinum · reductive elimination · supramolecular catalysis

[1] Y. Fang, J. A. Powell, E. Li, Q. Wang, Z. Perry, A. Kirchon, X. Yang, Z. Xiao, C. Zhu, L. Zhang, F. Huang, H.-C. Zhou, *Chem. Soc. Rev.* **2019**, *48*, 4707–4730.
[2] L. Zhao, X. Jing, X. Li, X. Guo, L. Zeng, C. He, C. Duan, *Coord. Chem. Rev.* **2019**, *378*, 151–187.
[3] P. Ballester, A. Scarso, *Front. Chem.* **2019**, *7*.
[4] C. Tan, D. Chu, X. Tang, Y. Liu, W. Xuan, Y. Cui, *Chem. Eur. J.* **2019**, *25*, 662–672.
[5] Q. Zhang, L. Catti, K. Tiefenbacher, *Acc. Chem. Res.* **2018**, *51*, 2107–2114.
[6] C. Deraedt, D. Astruc, *Coord. Chem. Rev.* **2016**, *324*, 106–122.
[7] W. Cullen, M. C. Misuraca, C. A. Hunter, N. H. Williams, M. D. Ward, *Nat. Chem.* **2016**, *8*, 231–236.
[8] S. H. A. M. Leenders, R. Gramage-Doria, B. de Bruin, J. N. H. Reek, *Chem. Soc. Rev.* **2015**, *44*, 433–448.
[9] S. Datta, M. L. Saha, P. J. Stang, *Acc. Chem. Res.* **2018**, *51*, 2047–2063.
[10] S. Pullen, G. H. Clever, *Acc. Chem. Res.* **2018**, *51*, 3052–3064.
[11] C. J. Brown, F. D. Toste, R. G. Bergman, K. N. Raymond, *Chem. Rev.* **2015**, *115*, 3012–3035.
[12] H. Amouri, C. Desmarets, J. Moussa, *Chem. Rev.* **2012**, *112*, 2015–2041.
[13] S. Ibáñez, M. Poyatos, E. Peris, *Acc. Chem. Res.* **2020**, *53*, 1401–1413.
[14] C. M. Hong, R. G. Bergman, K. N. Raymond, F. D. Toste, *Acc. Chem. Res.* **2018**, *51*, 2447–2455.
[15] H. Vardhan, F. Verpoort, *Adv. Synth. Catal.* **2015**, *357*, 1351–1368.
[16] D. L. Caulder, C. Brückner, R. E. Powers, S. König, T. N. Parac, J. A. Leary, K. N. Raymond, *J. Am. Chem. Soc.* **2002**, *123*, 8923–8938.
[17] M. Yoshizawa, M. Tamura, M. Fujita, *Science.* **2006**, *312*, 251–255.
[18] J. L. Bolliger, A. M. Belenguer, J. R. Nitschke, *Angew. Chem. Int. Ed.* **2013**, *52*, 7958–7962; *Angew. Chem.* **2013**, *125*, 8116–8120.
[19] V. Martí-Centelles, A. L. Lawrence, P. J. Lusby, *J. Am. Chem. Soc.* **2018**, *140*, 2862–2868.
[20] C. García-Simón, R. Gramage-Doria, S. Raoufmoghaddam, T. Parella, M. Costas, X. Ribas, J. N. H. Reek, *Am. Chem.* **2015**, *137*, 2680–2687.
[21] Z. Lu, R. Lavendomme, O. Burghaus, J. R. Nitschke, *Angew. Chem. Int. Ed.* **2019**, *58*, 9073–9077; *Angew. Chem.* **2019**, *131*, 9171–9175.
[22] D. M. Kaphan, M. D. Levin, R. G. Bergman, K. N. Raymond, F. D. Toste, *Science.* **2015**, *350*, 1235–1238.
[23] M. D. Pluth, R. G. Bergman, K. N. Raymond, *Science.* **2007**, *316*, 85–88.
[24] C. J. Hastings, M. D. Pluth, R. G. Bergman, K. N. Raymond, *J. Am. Chem. Soc.* **2010**, *132*, 6938–6940.
[25] Z. J. Wang, C. J. Brown, R. G. Bergman, K. N. Raymond, F. D. Toste, *J. Am. Chem. Soc.* **2011**, *133*, 7358–7360.

 © 2021 The Authors. Chemistry - A European Journal published by Wiley-VCH GmbH

[26] C. J. Brown, R. G. Bergman, K. N. Raymond, *J. Am, Chem. Soc.* **2009**, *131*, 17530–17531.
[27] D. H. Leung, R. G. Bergman, K. N. Raymond, *J. Am. Chem. Soc.* **2006**, *128*, 9781–9797.
[28] D. H. Leung, R. G. Bergman, K. N. Raymond, *J. Am. Chem. Soc.* **2007**, *129*, 2746–2747.
[29] M. D. Levin, D. M. Kaphan, C. M. Hong, R. G. Bergman, K. N. Raymond, F. D. Toste, *J. Am. Chem. Soc.* **2016**, *138*, 9682–9693.
[30] G. Norjmaa, J.-D. Maréchal, G. Ujaque, *J. Am. Chem. Soc.* **2019**, *141*, 13114–13123.
[31] G. Norjmaa, J.-D. Maréchal, G. Ujaque, *Chem. Eur. J.* **2020**, *26*, 6988–6992.
[32] V. V. Welborn, T. Head-Gordon, *J. Phys. Chem. Lett.* **2018**, *9*, 3814–3818.
[33] V. V. Welborn, T. Head-gordon, *Nat. Commun.* **2020**, *11*, 415.
[34] K. N. Houk, *Chem. Soc. Rev.* **2014**, *43*, 4905.
[35] D. J. Tantillo, *Acc. Chem. Res.* **2016**, *49*, 1079–1079.
[36] J. N. Harvey, F. Himo, F. Maseras, L. Perrin, *ACS Catal.* **2019**, *9*, 6803–6813.
[37] O. Eisenstein, G. Ujaque, A. Lledós, *Top. Organomet. Chem.* **2020**, 67, 1-38.
[38] P. Carlqvist, F. Maseras, *Chem. Commun.* **2007**, 748–750.
[39] S. P. Kim, A. G. Leach, K. N. Houk, *J. Org. Chem.* **2002**, *67*, 4250–4260.
[40] C. Goehry, M. Besora, F. Maseras, *ACS Catal.* **2015**, *5*, 2445–2451.
[41] H. Daver, J. N. Harvey, J. Rebek, F. Himo, *J. Am. Chem. Soc.* **2017**, *139*, 15494–15503.
[42] C. Goehry, M. Besora, F. Maseras, *Eur. J. Org. Chem.* **2018**, *2018*, 2103–2109.
[43] D. Chakraborty, P. K. Chattaraj, *J. Comput. Chem.* **2018**, *39*, 151–160.
[44] E. Pahima, Q. Zhang, K. Tiefenbacher, D. T. Major, *J. Am. Chem. Soc.* **2019**, *141*, 6234–6246.
[45] T. A. Young, V. Martí-Centelles, J. Wang, P. J. Lusby, F. Duarte, J. Am, *Chem. Soc.* **2020**, *142*, 1300–1310.
[46] L. Pesce, C. Perego, A. B. Grommet, R. Klajn, G. M. Pavan, *J. Am. Chem. Soc.* **2020**, *142*, 9792–9802.
[47] G. Sciortino, G. Norjmaa, J.-D. Maréchal, G. Ujaque, "Catalysis by Metal Organic Cages: A Computational Perspective". Supramolecular Catalysis-New Directions and Developments, ISBN 978-3-527-34902-9; van Leeuwen, W.N.M., Raynal, M., Eds; Wiley- VCH: Weinheim, 2022. ISBN 978-3-527-34902-9.
[48] K. Wang, X. Cai, W. Yao, D. Tang, R. Kataria, H. S. Ashbaugh, L. D. Byers, B. C. Gibb, *J. Am. Chem. Soc.* **2019**, *141*, 6740–6747.
[49] M. P. Frushicheva, S. Mukherjee, A. Warshel, *J. Phys. Chem. B* **2012**, *116*, 13353–13360.
[50] See Supporting Information.
[51] J. Contreras-Garcia, E. R. Johnson, S. Keinan, R. Chaudret, J.-P. Piquemal, D. N. Beratan, W. Yang, *J. Chem. Theory Comput.* **2011**, *7*, 625–632.
[52] E. R. Johnson, S. Keinan, P. Mori-Sanchez, J. Contreras-Garcia, A. J. Cohen, W. Yang, *J. Am. Chem. Soc.* **2010**, *132*, 6498–6506.
[53] A. D. Becke, *J. Chem. Phys.* **1993**, *98*, 5648–5652.
[54] C. Lee, W. Yang, R. G. Parr, *Phys. Rev. B* **1988**, *37*, 785–789.
[55] S. Grimme, J. Antony, S. Ehrlich, H. Krieg, *J. Chem. Phys.* **2010**, *132*, 154104–154119.
[56] Gaussian 09, Revision D.01, M. J. Frisch, G. W. Trucks, H. B. Schlegel, G. E. Scuseria, M. A. Robb, J. R. Cheeseman, G. Scalmani, V. Barone, B. Mennucci, G. A. Petersson, H. Nakatsuji, M. Caricato, X. Li, H. P. Hratchian, A. F. Izmaylov, J. Bloino, G. Zheng, J. L. Sonnenberg, M. Hada, M. Ehara, K. Toyota, R. Fukuda, J. Hasegawa, M. Ishida, T. Nakajima, Y. Honda, O. Kitao, H. Nakai, T. Vreven, J. A. Montgomery, Jr., J. E. Peralta, F. Ogliaro, M. Bearpark, J. J. Heyd, E. Brothers, K. N. Kudin, V. N. Staroverov, T. Keith, R. Kobayashi, J. Normand, K. Raghavachari, A. Rendell, J. C. Burant, S. S. Iyengar, J. Tomasi, M. Cossi, N. Rega, J. M. Millam, M. Klene, J. E. Knox, J. B. Cross, V. Bakken, C. Adamo, J. Jaramillo, R. Gomperts, R. E. Stratmann, O. Yazyev, A. J. Austin, R. Cammi, C. Pomelli, J. W. Ochterski, R. L. Martin, K. Morokuma, V. G. Zakrzewski, G. A. Voth, P. Salvador, J. J. Dannenberg, S. Dapprich, A. D. Daniels, O. Farkas, J. B. Foresman, J. V. Ortiz, J. Cioslowski, D. J. Fox, Gaussian, Inc., Wallingford CT, **2013**.
[57] A. W. Ehlers, M. Böhme, S. Dapprich, A. Gobbi, A. Höllwarth, V. Jonas, K. F. Köhler, R. Stegmann, A. Veldkamp, G. Frenking, *Chem. Phys. Lett.* **1993**, *208*, 111–114.
[58] A. Höllwarth, M. Böhme, S. Dapprich, A. W. Ehlers, A. Gobbi, V. Jonas, K. F. Köhler, R. Stegmann, A. Veldkamp, G. Frenking, *Chem. Phys. Lett.* **1993**, *208*, 237–240.
[59] A. V. Marenich, C. J. Cramer, D. G. Truhlar, *J. Phys. Chem. B* **2009**, *113*, 6378–6396.
[60] S. Grimme, *Chem. Eur. J.* **2012**, *18*, 9955–9964.
[61] V. S. Bryantsev, M. S. Diallo, W. A. Goddard, *J. Phys. Chem. B* **2008**, *112*, 9709–9719.
[62] D. A. Case, R. M. Betz, D. S. Cerutti, T. E. Cheatham, III, T. A. Darden, R. E. Duke, T. J. Giese, H. Gohlke, A. W. Goetz, N. Homeyer, S. Izadi, P. Janowski, J. Kaus, A. Kovalenko, T. S. Lee, S. LeGrand, P. Li, C. Lin, T. Luchko, R. Luo, B. Madej, D. Mermelstein, K. M. Merz, G. Monard, H. Nguyen, H. T. Nguyen, I. Omelyan, A. Onufriev, D. R. Roe, A. Roitberg, C. Sagui, C. L. Simmerling, W. M. Botello-Smith, J. Swails, R. C. Walker, J. Wang, R. M. Wolf, X. Wu, L. Xiao, P. A. Kollman (2016), AMBER **2016**, University of California, San Francisco.
[63] P. Li, K. M. Merz, *J. Chem. Inf. Model.* **2016**, *56*, 599–604.
[64] J. Wang, W. Wang, P. A. Kollman, D. A. Case, *J. Mol. Graphics Modell.* **2006**, *25*, 247–260.
[65] C. I. Bayly, P. Cieplak, W. D. Cornell, P. A. Kollman, *J. Phys. Chem.* **1993**, *97*, 10269–10280.
[66] G. Norjmaa, P. Vidossich, J.-D. Maréchal, G. Ujaque *J. Chem. Inf. Model.* **2021**, *61*, 4370-4381 https://doi.org/10.1021/acs.jcim.1c00348.
[67] J. Wang, R. M. Wolf, J. W. Caldwell, P. A. Kollman, D. A. Case, *J. Comput. Chem.* **2004**, *25*, 1157–1174.

Manuscript received: June 22, 2021
Accepted manuscript online: September 21, 2021
Version of record online: October 13, 2021

 © 2021 The Authors. Chemistry - A European Journal published by Wiley-VCH GmbH